Single-chip detector for electron spin resonance spectroscopy

T. Yalcin[1,2] and G. Boero[2,a)]
[1]*Hochschule für Technik und Architektur Luzern (HTA), 6048 Horw, Switzerland*
[2]*Ecole Polytechninque Federale de Lausanne (EPFL), 1015 Lausanne, Switzerland*

(Received 28 April 2008; accepted 22 July 2008; published online 30 September 2008)

We have realized an innovative integrated detector for electron spin resonance spectroscopy. The microsystem, consisting of an *LC* oscillator, a mixer, and a frequency division module, is integrated onto a single silicon chip using a conventional complementary metal-oxide-semiconductor technology. The implemented detection method is based on the measurement of the variation of the frequency of the integrated *LC* oscillator as a function of the applied static magnetic field, caused by the presence of a resonating sample placed over the inductor of the *LC*-tank circuit. The achieved room temperature spin sensitivity is about 10^{10} spins/GHz$^{1/2}$ with a sensitive volume of about $(100\ \mu\text{m})^3$. © *2008 American Institute of Physics.* [DOI: 10.1063/1.2969657]

I. INTRODUCTION

Electron spin resonance (ESR) is a powerful spectroscopic tool used in physics, chemistry, biology, medicine, and materials science.[1–4] Conventional ESR spectrometers essentially consist of a microwave source, a transmission/reception bridge, a resonator, and a detection arm, interconnected by coaxial cables or waveguides. The resonators are optimized for samples having a volume between 1 mm^3 and 1 cm^3. The achieved spin sensitivity is typically of the order 10^{10} spins/GHz$^{1/2}$ at 300 K (1 G=10^{-4} T).

Dielectric or ferroelectric inserts in standard cavities,[5,6] millimeter sized high dielectric constant ring resonators,[7] cavities with narrow slits for local measurements outside the cavity,[8] and small solenoidal and planar coils,[9–14] allow one to perform optimized experiments on samples having volumes down to $(100\ \mu\text{m})^3$, with spin sensitivities down to 10^9 spins/GHz$^{1/2}$. Noninductive detection methods,[15–21] such as the mechanical and optical techniques, have already achieved or can potentially achieve single-spin sensitivity. However, they still suffer from a limited versatility and, in most of the situations, they do not represent a valid alternative to the inductive approach.

In this paper we present an innovative ESR spectrometer based on the integration on a single silicon chip of the most important, sensitivity wise, excitation, and detection components (oscillator, excitation/detection microcoil, mixer, and frequency division module). The implemented inductive but unconventional detection method is inspired to some nuclear magnetic resonance and ESR spectrometers realized from the 1950s to 1980s.[22–28] In these spectrometers the coil (or the cavity) containing the sample determines the oscillation frequency of a positive feedback circuitry connected to them. The magnetic resonance is usually detected by measuring the variation of the amplitude of the oscillations as a function of the applied static magnetic field. Alternatively, the variation of the frequency of the oscillations can be measured, as demonstrated in the integrated microsystems described in this paper. The ESR phenomenon determines a change in the impedance of the integrated inductor *L*, which, in turns, determines a variation of the frequency of the integrated *LC* oscillator.

The aim of our work is the realization of single-chip high-sensitivity low-cost microsystems to perform optimized ESR experiments on sample having volumes of $(100\ \mu\text{m})^3$ and smaller. Particularly interesting is the possibility to fabricate a dense array of detectors on a single chip for parallel spectroscopy and imaging.

II. PRINCIPLE OF OPERATION

From the steady-state solution of the Bloch equation, the susceptibility of an ESR sample having a single homogeneously broadened line placed in a static magnetic field $B_0\hat{\mathbf{z}}$ and a microwave magnetic field $2B_1 \cos \omega t\hat{\mathbf{x}}$ can be written as[4]

$$\chi' = -\frac{1}{2}\frac{\Delta\omega T_2^2}{1+(T_2\Delta\omega)^2+\gamma^2 B_1^2 T_1 T_2}\omega_0\chi_0,$$

$$\chi'' = \frac{1}{2}\frac{T_2}{1+(T_2\Delta\omega)^2+\gamma^2 B_1^2 T_1 T_2}\omega_0\chi_0, \tag{1}$$

where $\chi=\chi'-j\chi''$ is the sample complex susceptibility, $\Delta\omega=\omega-\omega_0$, $\omega_0=\gamma B_0$, T_1 is longitudinal relaxation time, T_2 is the transversal relaxation time, and χ_0 is the static susceptibility. For a spin 1/2 system with $g=2$ we have $\chi_0=(\mu_0 N\gamma^2\hbar^2/4kT)$, where N is the spin density (in m^{-3}), and T is the sample temperature (in kelvins).

The impedance of a coil filled with a material having susceptibility χ is

$$Z_\chi = j\omega L(1+\eta\chi)+R = j\omega L_\chi + R_\chi, \tag{2}$$

where $L_\chi=L+L\eta\chi'$ and $R_\chi=R+\omega L\eta\chi''$. *L* and *R* are the inductance and the resistance of the coil without the sample, respectively. The filling factor η is given by

a)Electronic mail: giovanni.boero@epfl.ch.

$$\eta = \left(\int_{V_s} |\mathbf{B}_u(\mathbf{x})|^2 dV \Big/ \int_{V} |\mathbf{B}_u(\mathbf{x})|^2 dV \right) \cong (V_s/V_c), \quad (3)$$

where V_s is the sample volume, V is the entire space, V_c is the sensitive volume of the coil, $\mathbf{B}_u$ is the field produced by a unitary current in the coil (in T/A), and $\mathbf{x}$ is the position vector in the volumes V_s and V. For $\omega \cong \omega_0$, the presence of the sample modifies both the reactive as well as the resistive part of the coil impedance.

The resonance frequency of an LC oscillator (with losses dominated by the series resistance of the coil) is

$$\omega_{LC\chi} = \frac{1}{\sqrt{L_\chi C}} \sqrt{1 - \frac{R_\chi^2 C}{4L_\chi}} = \frac{\omega_{LC}}{\sqrt{1+\eta\chi'}} \sqrt{1 - \frac{1}{4Q} \frac{(1+Q\eta\chi'')^2}{1+\eta\chi'}}, \quad (4)$$

where $\omega_{LC} \equiv (1/\sqrt{LC})$ and $Q \equiv (\omega_{LC} L/R)$. In typical experimental conditions we have that $\eta\chi' \ll 1$, $\eta\chi'' \ll 1$, and $Q \gg 1$. In these conditions, it can be shown that the variation of the oscillator frequency due to the magnetic resonance of the sample is

$$\Delta\omega_{LC} \equiv \omega_{LC\chi} - \omega_{LC} \sqrt{1 - \frac{R^2 C}{4L}} \cong \frac{1}{2} \omega_{LC} \eta\chi'. \quad (5)$$

The maximum variation of the oscillator frequency, which occurs for $\gamma^2 B_1^2 T_1 T_2 \ll 1$ and $T_2 \Delta\omega = \pm 1$, is $(\Delta\omega_{LC})_{\max} \cong \pm (1/8) \omega_0^2 T_2 \eta\chi_0$.

In order to estimate the achievable signal-to-noise ratio and spin sensitivity, we have to compute the expected frequency noise. The root-mean-square value of the frequency fluctuations for a detection bandwidth Δf of an ideal LC oscillator (i.e., with phase noise dominated by the thermal noise of the coil series resistance R) can be written as[25]

$$\Delta\omega_{LC,\text{noise}} = \sqrt{\frac{kTR\omega_{LC}^2 \Delta f}{V_0^2}}, \quad (6)$$

where V_0 is the oscillator voltage amplitude.

Assuming that the frequency variation is given by Eq. (5), the signal-to-noise ratio is

$$\text{SNR} \equiv \frac{2\Delta\omega_{LC}}{3\Delta\omega_{LC,\text{noise}}} = \frac{1}{3} \frac{\eta\chi' V_0}{\sqrt{kTR\Delta f}}. \quad (7)$$

The factor 2 is introduced to consider the peak-to-peak frequency variation whereas the factor 3 is introduced, quite arbitrarily, to take into consideration that when the signal peak-to-peak amplitude is equal to the root mean square of the noise, the signal cannot be readily distinguished from the noise.

The oscillator voltage amplitude V_0, for $Q \gg 1$, can be written as

$$V_0 \cong I\omega_{LC} L \cong \frac{2B_1}{B_u} \omega_{LC} \frac{B_u^2 V_c}{\mu_0} = 2B_1 \omega_{LC} \frac{B_u V_c}{\mu_0}, \quad (8)$$

where I is the microwave current in the coil. If the oscillator voltage amplitude V_0 is increased in order to reduce the phase noise, B_1 is also increased. Consequently, χ' and $\Delta\omega_{LC}$ are reduced [see Eqs. (1) and (5)], and the resonance line broadened. From Eqs. (7) and (8) we have that the signal-to-noise ratio is

$$\text{SNR} \cong \frac{2}{3} \frac{\omega_{LC} B_u V_s}{\mu_0 \sqrt{kTR\Delta f}} \chi' B_1. \quad (9)$$

The product $\chi' B_1$ grows with B_1 reaching asymptotically the maximum value $(\chi' B_1)_{\max} = (1/4)\chi_0 B_0 \sqrt{T_2/T_1}$. Hence, for $T_1 = T_2$, we have

$$\text{SNR} \cong \frac{1}{6} \frac{\omega_{LC} B_u V_s}{\mu_0 \sqrt{kTR\Delta f}} \chi_0 B_0, \quad (10)$$

and the spin sensitivity (in spins/$\text{Hz}^{1/2}$) is

$$N_{\min} \equiv \frac{1}{\text{SNR}} \frac{NV_s}{\sqrt{\Delta f}} \cong \alpha \frac{T^{3/2}\sqrt{R}}{B_0^2 B_u}, \quad (11)$$

where $\alpha = 24 k^{3/2} \gamma^{-3} \hbar^{-2} \cong 20\ \text{m}^{-1}\ \text{kg}^{5/2}\ \text{s}^{-4}\ \text{K}^{-3/2}\ \text{A}^{-3}$.

The spin sensitivity given in Eq. (11) is identical to that obtained for the conventional "induced voltage" method [see Eq. (6) in Ref. 13]. The induced voltage is dependent on the precessing magnetization amplitude whereas the oscillator frequency variation depends on the complex susceptibility amplitude (and, consequently, they have a different dependence on B_1). However, the noise for the induced voltage method is independent of B_1 whereas for the oscillator frequency variation method is linearly proportional to B_1 (through the dependence on V_0). This explains qualitatively why the theoretically achievable spin sensitivities are identical.

If we consider a single-turn coil having a diameter $d = 100\ \mu\text{m}$ and a resistance $R = 1\ \Omega$, operating at $\omega_0 = 2\pi \times 9$ GHz and $T = 300$ K, we have $B_u \cong (\mu_0/d) = 0.013$ T/A and $N_{\min} \cong 10^8$ spins/$\text{Hz}^{1/2}$.

III. DESCRIPTION OF THE INTEGRATED MICROSYSTEM

Figure 1 shows a schematic view of the integrated microsystem, which consists of two LC-tank voltage-controlled oscillators (VCOs), a mixer, a filter amplifier, and two frequency dividers. Details of the integrated subcircuits are shown in Fig. 2. The circuit has been realized using the 0.35 μm digital complementary metal-oxide-semiconductor (CMOS) process offered by AMI Semiconductors. The total chip area is 1 mm^2.

We have integrated two VCOs instead of one to facilitate the first downconversion of the oscillator frequency, which can be performed by a simple mixer instead of a more complicated microwave frequency divider. The VCOs have been implemented as differential negative resistance oscillators.[29] The inductors of the two LC-tank circuits are identical. The VCO frequencies are set to two different values using the two pairs of nonidentical n-type MOS varactors. Since the two varactors are different, even when the same control voltage is applied to both varactors (i.e., $SA = SB$), the capacitance values are different. The approximately rectangular VCO coils are placed orthogonally one with respect to the other. The magnetic coupling between the two coils is ideally zero and, consequently, the risk of injection locking between the two VCOs is significantly reduced. Each coil has a di-

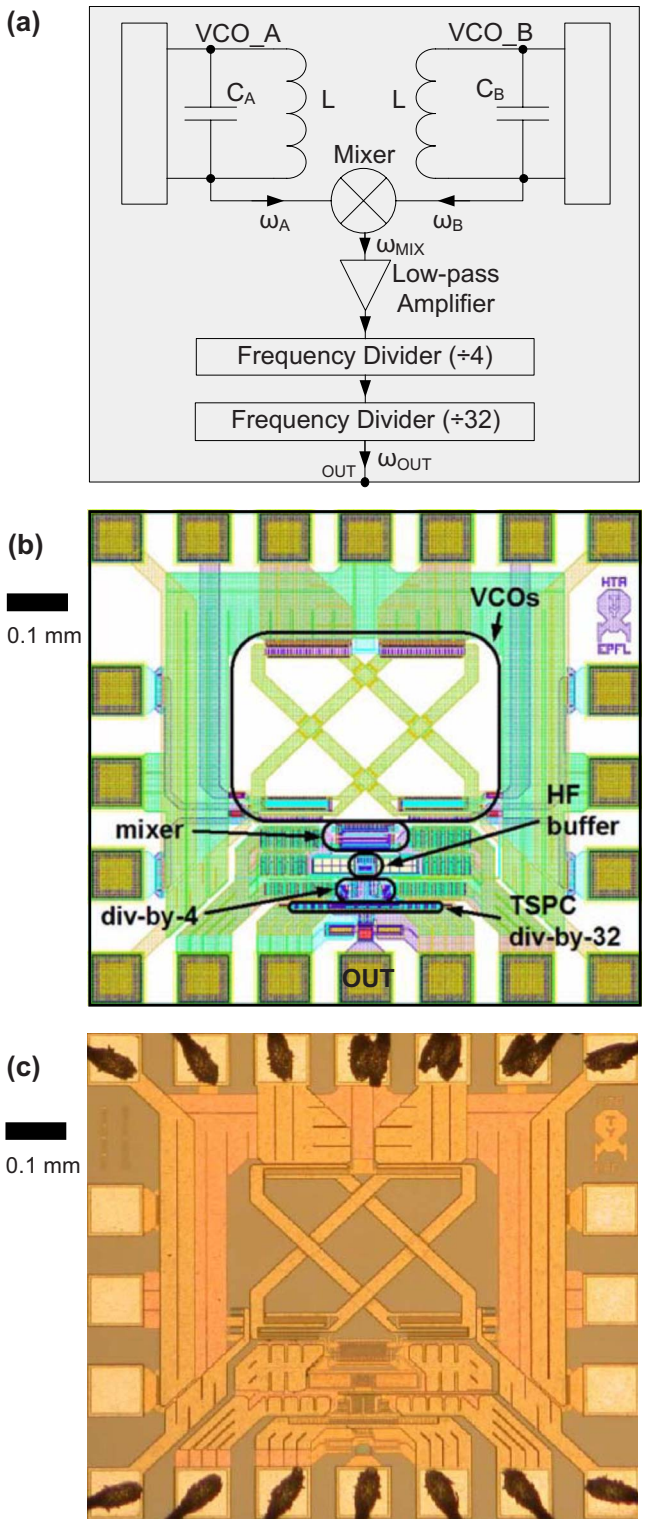

FIG. 1. (Color online) (a) Block diagram, (b) layout, and (c) picture of the realized chip.

mension of about 300×100 μm^2, with a metal (aluminum) thickness of 2 μm and width of 20 μm. The mixer, based on the standard Gilbert topology,[29] is used to obtain a signal at frequency $\omega_{mix}=\omega_A-\omega_B$, i.e., at the difference of the two VCO frequencies. A low pass filter amplifier is designed at the mixer output for the suppression of the sum frequency component. The frequency division is implemented in two stages: a high frequency divide-by-4 block, and a low frequency divide-by-32 block. The high frequency divider is based on the topology presented in Ref. 30. The low frequency divider is realized connecting five identical divide-by-2 circuits, implemented using single-ended true-single-phase-clocked flip flops.[31] Consequently, the frequency at the output of the integrated circuit is $\omega_{out}=(\omega_A-\omega_B)/128$. When the external static magnetic field B_0 sets the Larmor frequency close to the center frequency of one of the VCOs, the center frequency of the concerned VCO changes according to Eq. (4). Since the two VCO have different frequencies, the resonance conditions are fulfilled twice as B_0 is swept. Therefore, the frequency ω_{out} also changes twice.

IV. INTEGRATED MICROSYSTEM PERFORMANCE

Figure 3(a) shows a schematic of the apparatus used to investigate the performance of the realized ESR microsystem. The employed homebuilt and commercial components are mentioned in the figure caption. The integrated microsystem is introduced in the electromagnet, equipped also with field modulation coils. The chip can operate at supply voltages from 2.0 to 3.6 V, with best signal-to-noise ratio at 2.2 V. From linewidth broadening experiments, we estimate that $B_1\cong0.4$ mT at the center of the coils at a supply voltage of 2.2 V. The temperature of the chip, measured by an infrared thermometer, is about 305 K at 2.2 V (the supply current is 74 mA and, hence, the power consumption of the chip is 160 mW). The ambient temperature is 298 K. With the varactors control voltages and supply voltage all set to 2.2 V, the frequencies of the two integrated VCOs are $\omega_A\cong2\pi\times8.4$ GHz and $\omega_B\cong2\pi\times9.4$ GHz, respectively. At the output of the chip, we have a signal at frequency $\omega_{out}=(\omega_A-\omega_B)/128\cong2\pi\times7.4$ MHz, with peak-to-peak amplitude of about 2 V.

Due to the limited current capabilities of the integrated circuit, the signal at the output of the chip is introduced in an inverter buffer. The output of the buffer is mixed with a local oscillator signal at 7.6 MHz. The signal at the output of the mixer (at 200 kHz) is introduced in a phase-locked-loop (PLL) circuitry for frequency-to-voltage conversion. The signal at the output of the PLL is demodulated by a lock-in amplifier. The lock-in internal reference signal is amplified and delivered to the field modulation coil.

The spin sensitivity of the realized microsystem is evaluated by measuring the signal-to-noise ratio obtained with a sample of 1,1-diphenyl-2-picryl-hydrazyl (DPPH) (Sigma D9132) with a volume of about $(14\ \mu m)^3$. The sample is placed approximately in the center of the square shaped common area of the two rectangular coils. The obtained spectrum is shown in Fig. 4(a) (the experimental conditions are specified in the figure caption).

Due to the field modulation, the shape of the signals is approximately equal to the derivative of a dispersionlike curve.[4] The two signals obtained by sweeping the static magnetic field have opposite sign, as expected because we are measuring the difference of the frequency of the two VCO (and not directly the frequency variation of each VCO). The measured signal-to-noise ratio [as defined by Eq. (8)] is about 120 (the frequency variation is about 17 kHz and the

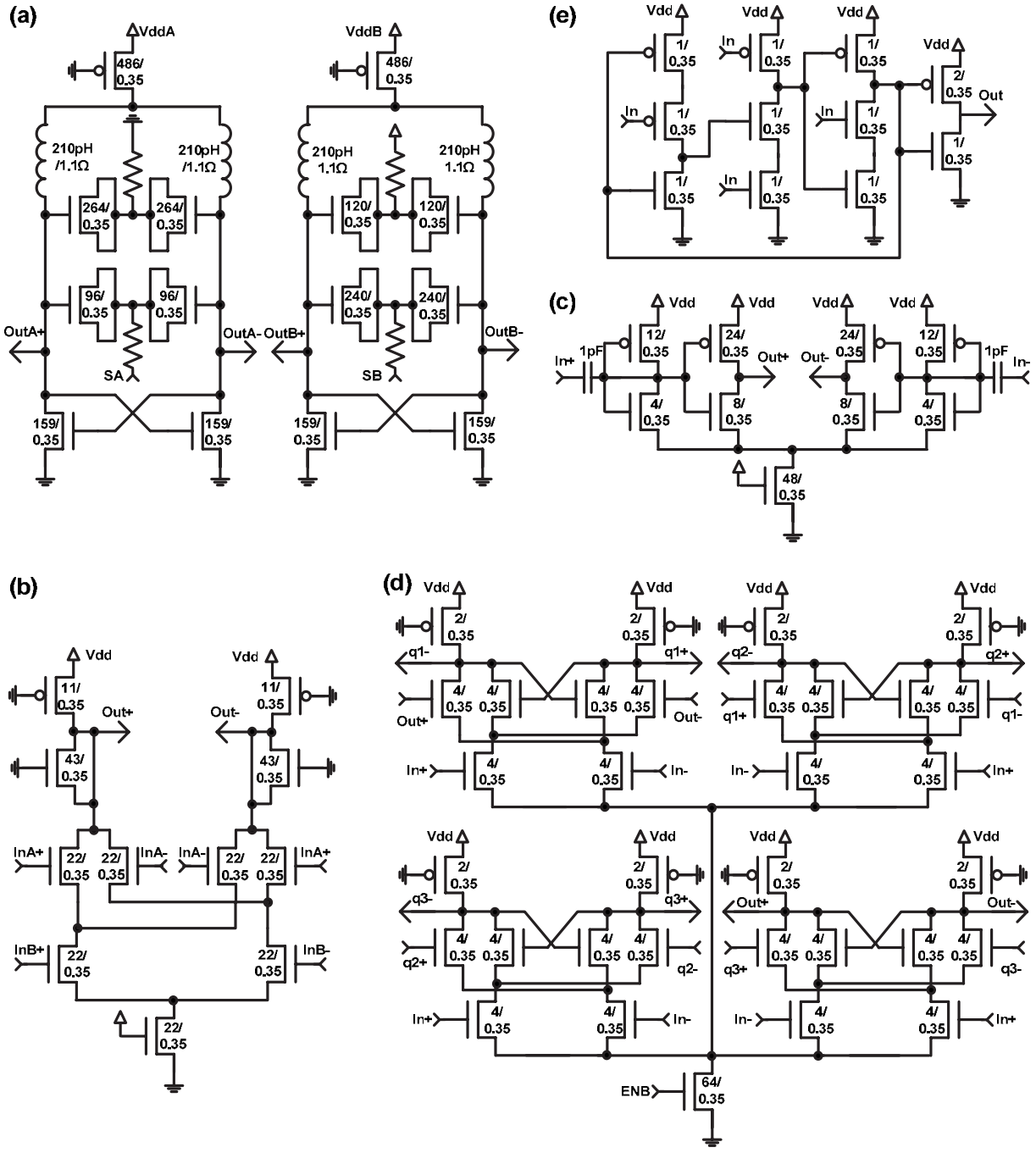

FIG. 2. Schematics of the integrated electronics. In the measurements presented in this paper we set $V\mathrm{dd}=V\mathrm{ddA}=V\mathrm{ddB}=SA=SB=E\mathrm{NB}=2.2$ V. The transistors dimensions are indicated in micrometers. (a) VCOs. (b) Mixer. (c) Low pass filter amplifier (HF buffer). (d) Frequency divider (divide-by-4). (e) Frequency divider (divide-by-2).

root mean square of the noise is about 47 Hz). Since in our experimental conditions $N \cong 2\times 10^{27}$ spins/m^3 and $\Delta f = 2.5$ Hz, the experimental spin sensitivities [as defined by Eq. (11)] is about $N_{\min} \cong 3\times 10^{10}$ spins/Hz$^{1/2}$ (i.e., about 1.5×10^{10} spins/GHz$^{1/2}$, since the natural linewidth of DPPH is about 2 G).

As shown in Fig. 4(a), the experimental amplitude of the two signals corresponding to the two VCOs is not the same (i.e., 17 and 14 kHz, respectively). Figure 4(b) shows the signals computed numerically from Eq. (4) using the parameters specified in the caption. Contrary to the measured amplitude, the computed signal amplitude corresponding to the higher oscillator frequency is larger [as expected from Eqs. (1) and (5) due to the larger susceptibility χ' and operating frequency ω_{LC}]. Additionally, the shape of the measured signals are not perfectly matched to those in Fig. 4(b). Nevertheless, the quantitative agreement between measured and computed signal amplitudes and shapes is sufficiently good to consider Eq. (4) as a valid approximation of the behavior of the microsystem.

From Eq. (5), the maximum peak-to-peak variation, for $\gamma^2 B_1^2 T_1 T_2 \ll 1$ and $\eta \cong 3\times 10^{-4}$, is about $2\Delta\omega_{LC} \cong 2\pi \times 130$ kHz. In our experimental conditions, we have measured a signal which is almost a factor 10 smaller (i.e., 2π

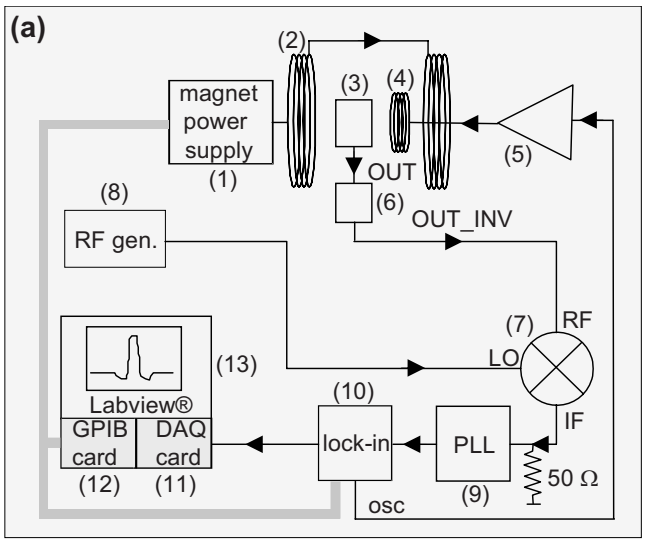

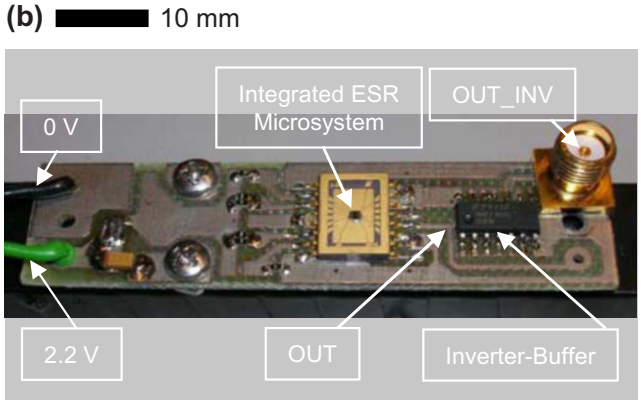

FIG. 3. (Color online) (a) Schematic of the experimental setup. (1) Electromagnet power supply (Bruker, 0–150 A). (2) Electromagnet (Bruker, 0–2 T). (3) Integrated ESR microsystem. (4) Magnetic field modulation coil. (5) Power amplifier (Rohrer PA508). (6) Inverter buffer (Fairchild MM74HC04). (7) Mixer (Mini-Circuits ZAD-3). (8) Signal generator (HP 33120A). (9) PLL circuit (National Semiconductor LM565CN followed by an operational amplifier Analog Devices AD829JN). The PLL circuit has a central frequency of 200 kHz, a bandwidth of 20 kHz, and a sensitivity of 0.1 mV/Hz. (10) Lock-in amplifier (EG&G 7265). (11) Data acquisition card (National Instruments DAQPad-6015-USB). (12) GPIB card (National Instruments GPIB-USB-HS). (13) Labview-based software (National Instruments) on a Windows-XP personal computer. (b) Picture of the printed circuit board used to interface the chip with the external electronics.

$\times 17$ kHz). This results, quite accurately predicted by Eq. (4) and shown in Fig. 4(b), is due to (a) the large B_1 field ($B_1 \cong 0.4$ mT) produced by the integrated oscillators which broadens the line and decreases the frequency variation, (b) the nonoptimal modulation amplitude $B_m \cong 0.2$ mT (in our condition of broadened line the optimal value for the modulation amplitude for optimal signal-to-noise ratio would be about 0.4 mT).

In our experiments, as in common continuous wave ESR experiments, we have added a magnetic field at kilohertz frequencies to the static magnetic field in order to improve the signal-to-noise ratio. The effective noise measured at the modulation frequency (i.e., at about 20 kHz) corresponds to about 30 $\mathrm{Hz/Hz^{1/2}}$ at the *LC*-oscillator output, which is about one order of magnitude larger than the noise of an ideal *LC* oscillator computed from Eq. (6) assuming *R*

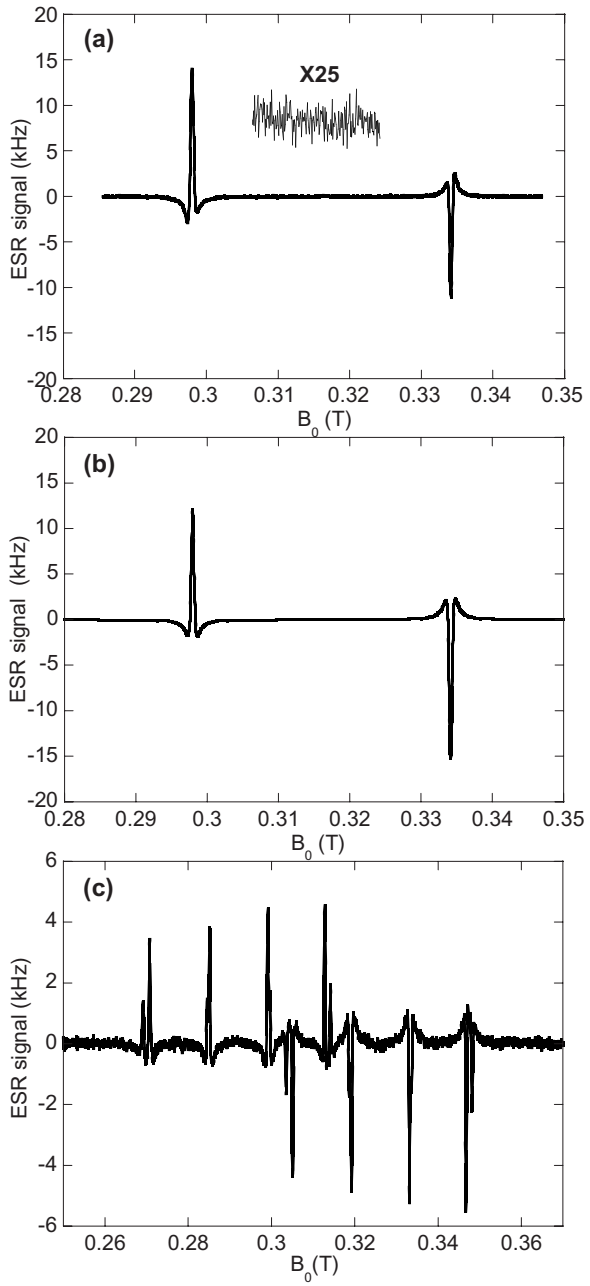

FIG. 4. ESR spectra. The experimental ESR signal shown here (in kHz) is the amplitudes of the component at the field modulation frequency of the difference between the two *LC*-oscillator frequencies $\omega_A - \omega_B$, computed from the experimental signals (in V) obtained at the output of the lock-in amplifier considering: the lock-in gain (500), the PLL frequency-to-voltage conversion factor (0.1 mV/Hz), and the integrated frequency division (128) (i.e., a global conversion factor of 2560 Hz/V). (a) Measured spectrum with a DPPH sample having a volume of $(14\ \mu\mathrm{m})^3$. Experimental conditions: temperature $T=305$ K, microwave magnetic field $B_1 \cong 0.4$ mT, magnetic field modulation amplitude $B_m \cong 0.2$ mT, magnetic field modulation frequency $\nu_m=21$ kHz, sweep time $t_s=400$ s, lock-in equivalent noise bandwidth $\Delta f \cong 2.5$ Hz (time constant $\tau_c=100$ ms, filter slope $s_f=6$ dB/octave). (b) Simulated spectrum with a DPPH sample having a volume of $(14\ \mu\mathrm{m})^3$. The spectrum is computed numerically from Eq. (4). Simulation parameters are $T=305$ K, $B_1=0.4$ mT, $B_m=0.2$ mT, $\eta=0.3\times10^{-3}$ [computed numerically from Eq. (3)], $Q=10$, $N=2\times10^{27}\ \mathrm{m^{-3}}$, $T_1=T_2=62$ ns, $\omega_{LC,A}=8.4$ GHz, $\omega_{LC,B}=9.4$ GHz. (c) Measured spectrum with a $\mathrm{Cu(mnt)_2}$ in $\mathrm{Ni(mnt)_2}$ (copper concentration of 1%) sample having a volume of $(100\ \mu\mathrm{m})^3$. Experimental conditions (see notations above): $T=305$ K, $B_1 \cong 0.4$ mT, $B_m \cong 0.2$ mT, $\nu_m=5.3$ kHz, $t_s=500$ s, $\Delta f \cong 2.5$ Hz ($\tau_c=100$ ms, $s_f=6$ dB/octave).

$=2\ \Omega$ and $V_0=2$ V (the contribution to the measured noise from the external mixer, PLL circuitry, and lock-in amplifier is negligible). We have observed that the noise achieves a minimum value at the limit of the bandwidth of our external PLL circuitry (i.e., about 20 kHz). Measurements of the phase noise spectral density indicate that we could reduce the noise by a factor of 3 (i.e., down to 10 $\mathrm{Hz}/\mathrm{Hz}^{1/2}$) modulating at a frequency of 100 kHz instead of 20 kHz. Unfortunately, our present setup does not allows us to increase the modulation frequency above 20 kHz.

Figure 4(c) shows the ESR spectra obtained from of a single crystal of tetramethylammonium bis(maleonitriledithiolato)copper(II) ($Cu(mnt)_2$) in $Ni(mnt)_2$ with a copper concentration of about 1%. This measurement is reported to demonstrate that the spin sensitivity of the realized microsystems allows one to perform experiments on samples with low spin concentration and multiline spectrum.

V. DISCUSSION

As pointed out in Sec. II, the induced voltage and oscillator frequency variation methods have very similar theoretical spin sensitivities. In order to determine which of the two methods can practically achieve a better spin sensitivity, we have to evaluate in which case the assumption that the overall noise level is determined by the thermal noise of the coil resistance is more realistic. At frequencies below 1 GHz, it is a reasonable assumption for well designed "induced voltage" systems but not necessarily for "frequency variation" systems, where the positive feedback electronics might introduce significant additional noise. On the other hand, at 10 GHz and above, the design of low-noise preamplifiers and analog mixers might be problematic, especially using low-cost CMOS technologies.

Our future work will be focused on the improvement of the spin sensitivity of integrated ESR microsystems by a systematic investigation of the noise sources, and eventually, by an increase in the operating frequency and by a reduction in the sensitive volume [e.g., down to $(10\ \mu\mathrm{m})^3$]. Submicrometer silicon based technologies will be compared in terms of cost, achievable spin sensitivity, maximum operating frequency, and possibilities to integrate dense arrays and additional electronics (such as PLL circuits). Integrated *LC* oscillators operating up to 100 GHz, implemented using conventional CMOS and SiGe:BiCMOS technologies have been already reported,[32] suggesting a possible solution to improve the spin sensitivity by two orders of magnitude with respect to our present microsystem operating at 9 GHz.

[1] C. P. Poole, *Electron Spin Resonance* (Wiley, New York, 1983).
[2] A. Schweiger and G. Jeschke, *Principles of Pulse Electron Paramagnetic Resonance* (Oxford University Press, Oxford, 2001).
[3] J. A. Weil and J. R. Bolton, *Electron Paramagnetic Resonance* (Wiley, New York, 2007).
[4] A. Abragam, *Principles of Nuclear Magnetism* (Oxford University Press, Oxford, 1994).
[5] Y. E. Nesmelov, J. T. Surek, and D. D. Thomas, J. Magn. Reson. **153**, 7 (2001).
[6] E. M. Ganapolskii and L. Ya. Matsakov, Instrum. Exp. Tech. **38**, 746 (1995).
[7] A. Blank, C. R. Dunnam, P. P. Borbat, and J. H. Freed, Rev. Sci. Instrum. **75**, 3050 (2004).
[8] F. Sakram, A. Copty, M. Golosovsky, N. Bontemps, D. Davidov, and A. Frenkel, Appl. Phys. Lett. **82**, 1479 (2003).
[9] A. G. Webb, Prog. Nucl. Magn. Reson. Spectrosc. **31**, 1 (1997).
[10] Y. Morita and K. Ohno, J. Magn. Reson., Ser. A **102**, 344 (1993).
[11] K. Ohno and T. Murakami, J. Magn. Reson. (1969-1992) **79**, 343 (1988).
[12] H. Mahdjour, W. G. Clark, and K. Baberschke, Rev. Sci. Instrum. **57**, 1100 (1986).
[13] G. Boero, M. Bouterfas, C. Massin, F. Vincent, P.-A. Besse, R. S. Popovic, and A. Schweiger, Rev. Sci. Instrum. **74**, 4794 (2003).
[14] R. Narkowicz, D. Suter, and R. Stonies, J. Magn. Reson. **175**, 275 (2005).
[15] J. Gallop, P. W. Josephs-Franks, J. Davies, L. Hao, and J. Macfarlane, Physica C **368**, 109 (2002).
[16] G. Boero, P.-A. Besse, and R. S. Popovic, Appl. Phys. Lett. **79**, 1498 (2001).
[17] Y. Manassen, R. J. Hamers, J. E. Demuth, and A. J. Castellano, Phys. Rev. Lett. **62**, 2531 (1989).
[18] J. Wrachtrup, C. Vonborczyskowski, J. Bernard, M. Orrit, and R. Brown, Nature (London) **363**, 244 (1993).
[19] J. Köhler, Phys. Rep. **310**, 261 (1999).
[20] D. Rugar, C. S. Yannoni, and J. A. Sidles, Nature (London) **360**, 563 (1992).
[21] D. Rugar, R. Budakian, H. J. Mamin, and B. W. Chui, Nature (London) **430**, 329 (2004).
[22] R. V. Pond and W. D. Knight, Rev. Sci. Instrum. **21**, 219 (1950).
[23] F. N. H. Robinson, J. Sci. Instrum. **36**, 481 (1959).
[24] R. A. Wind, J. Phys. E **3**, 31 (1970).
[25] M. R. Smith and D. G. Hughes, J. Phys. E **4**, 725 (1971).
[26] W. M. Walsh and L. W. Rupp, Rev. Sci. Instrum. **41**, 1316 (1970).
[27] W. M. Walsh and L. W. Rupp, Rev. Sci. Instrum. **42**, 468 (1971).
[28] W. M. Walsh and L. W. Rupp, Rev. Sci. Instrum. **52**, 1029 (1981).
[29] T. H. Lee, *The Design of CMOS Radio-frequency Integrated Circuits* (Cambridge University Press, New York, 2004).
[30] C. M. Hung, B. A. Floyd, N. Park, and K. K. O, IEEE Trans. Microwave Theory Tech. **49**, 17 (2001).
[31] J. Yuan and C. Svensson, IEEE J. Solid-State Circuits **24**, 62 (1989).
[32] C. Cao and K. K. O, IEEE J. Solid-State Circuits **41**, 1297 (2006).